

# Yielding and Strain Stiffening in Entangled Assemblies of Frictional Granular Chains

M. Reza Shaebani<sup>1</sup> and Mehdi Habibi<sup>2</sup>

<sup>1</sup>*Department of Theoretical Physics and Center for Biophysics,  
Saarland University, 66123 Saarbrücken, Germany*

<sup>2</sup>*Laboratory of Physics and Physical Chemistry of Foods,  
Wageningen University, 6708WG Wageningen, The Netherlands*

Packings of macroscopic granular chains capture some of the essential aspects of molecular polymer systems and have been suggested as a paradigm to understand the physics on a molecular scale. However, here we demonstrate that the interparticle friction  $\mu$  in granular chain packings, which has no counterpart in polymer systems, leads to a nontrivial yielding and rheological response. Based on discrete element simulations we study the nonlinear rheology of random packings of granular chains under large amplitude oscillatory shear. We find that the maximum stress and the penetration depth of the shear deformation into the material bulk are nonmonotonic functions of friction with extrema at intermediate values of  $\mu$ . We also show that the regularly repeated gaps between the adjacent grains, which are special to commercial granular chains, broaden the shear zone and enhance the entanglements in the system by promoting the interlocking events between chains. These topological constraints can significantly increase the degree of strain stiffening. Our findings highlight the differences between the physics of granular chain packings and molecular polymer systems.

Polymer assemblies are key components of a variety of natural and synthetic materials [1]. Whereas many properties of these materials can be understood from the microscopic states and configurations of their constituent polymeric elements, it is technically very difficult to probe such microstructures directly. As a promising alternative, macroscale granular chains have been offered due to their analogies to polymer systems (e.g. chain stiffness- or length-dependence of the mechanical response, similar roles of packing fraction and temperature in jamming transition, etc.) [2–7]; but even the physics of macroscale disordered assemblies of long semiflexible objects has remained largely unexplored. The presence of topological constraints in these systems [6–13] leads to intriguing phenomena, such as strain stiffening under shear [6–8], and makes them different from, e.g., packings of rods where particle elongation and volume exclusion govern the behavior. Understanding the yielding, flow, and stiffening of entangled athermal systems of semiflexible chains is crucial to uncover the underlying structure of natural filamentous assemblies, such as bird nests [14], and for design of disordered meta materials [15–18] and new smart textiles [18–22].

How different entanglement mechanisms—such as interlocking events between chains [7] or formation of semiloops [6]—contribute to the overall mechanical response has remained unclear, which is crucial to develop a quantitative theory of yielding and stiffening of entangled chain packings. More importantly, the presence of frictional interactions increases the complexity of the problem on the macroscale compared to molecular polymer systems. While the impact of friction on the structure and dynamics of granular systems has been extensively studied [23–31], a detailed understanding of how the interplay between topological constraints and interparticle friction governs the mechanical response of chain

packings is currently lacking. Furthermore, much less is known about the nonlinear rheology of these systems when yielding under shear [32]. Rheological response of dissipative systems to an oscillatory shear has been of particular interest [33–36]. How far the shear-induced deformation penetrates into the bulk of granular-chain packings and what role the key factors, particularly friction and entanglements, play are intriguing problems [8].

Here, we numerically study the response of frictional granular-chain packings to large amplitude oscillatory shear (LAOS); see Fig. 1. By measuring the steady-state maximum stress and the penetration depth of the shear deformation into the material bulk, we find that the mechanical and rheological responses of chain packings show

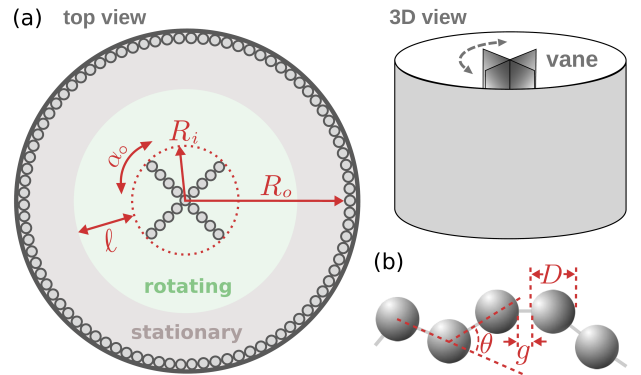


FIG. 1. (a) Schematic of the simulation setup. The four-blade vane of radius  $R_i$  rotates with an amplitude  $\alpha_o$  inside a cylindrical container of radius  $R_o$  filled with granular chains. Background colors illustrate the rotating inner part and the stationary outer region, with the border defining the penetration depth  $\ell$ . (b) Illustration of the granular chains composed of spherical grains of diameter  $D$ . A constant gap  $g$  is imposed (as a bond) between the neighboring grains along the chain. The bond angle  $\theta$  can vary within the  $0 \leq \theta \leq \theta_{\max}$  range.

nonmonotonic dependencies on the coefficient of friction  $\mu$ . The competition between a higher connectivity of the contact network at low  $\mu$  and a larger local freedom for the tangential frictional forces at high  $\mu$  leads to the highest stability at intermediate values of  $\mu$ . We also disentangle the contribution of interlocking and semiloops to the rheological response and show that the presence of regular gaps  $g$  along commercially available granular chains can enhance the degree of strain stiffening.

We consider a packing of granular chains inside a cylindrical container where a rotating four-blade vane applies a sinusoidal deformation  $\alpha = \alpha_o \sin(2\pi ft)$ . The rotation frequency is set to  $f = 0.1$  Hz and the rotation amplitude satisfies  $\alpha_o \geq 10^\circ$  (corresponding to shear strains  $\gamma \gtrsim 0.17$ ) in all simulations to remain in the LAOS regime [8]. We use the contact dynamics (CD) method for rigid particles [37] to perform large-scale parallel simulations [38]. The unit of the length is set to the diameter  $D$  of the spherical grains which are used to construct the chains and rigid blades and to roughen the container surfaces to avoid slip. The radii of the blades and container are  $R_i = 4.5D$  and  $R_o = 25D$ , respectively. To construct the chains we impose a gap  $g$  between the surfaces of adjacent grains, as if there is a rigid bond between them; thus, the distance between the successive grain centers along the chain is  $g + D$  as shown in Fig. 1. The concept of introducing a fixed gap size is suited very well to the CD method where the interparticle forces are handled as constraint forces [37, 39]. We vary  $g$  in our simulations but it is restricted to  $g \leq 0.4D$  to keep the adjacent grains close enough to each other such that the imaginary bonds never touch. The angle  $\theta$  between the successive imaginary bonds is flexible to vary within the  $0 \leq \theta \leq \theta_{\max} = 40^\circ$  range. One can assign a local persistence length  $\ell_p$  to the chain, deduced from the local directional persistence  $p = \cos(\theta)$  via  $p = e^{-\ell/\ell_p}$  [5, 40, 41].

First, the shear cell is loaded with chains of equal length  $N$  up to the height  $h \approx 25D$  and the packing is relaxed into equilibrium under gravity. We construct a new packing for each value of the interparticle friction  $\mu$ . The oscillatory shear deformation in the LAOS regime is then performed and the stress and strain are measured after each  $0.1^\circ$  change in the deflection angle. We previously proved that the numerical predictions of our simulation method are in quantitative agreement with the experimental results under similar conditions [8].

*Penetration depth of the deformations.*— While the material at the central part of the cell rotates with the blades, the movements beyond the blade edges decay with the distance from the moving boundary. Typical angular velocity profiles shown in Fig. 2(a) indicate that increasing the chain length  $N$  leads to larger fluctuations of the velocity profile, since the yielding domain depends stronger on the initial packing configuration. Moreover, increasing  $N$  enhances the size of the shear zone. Wide shear zones away from the boundaries were previously

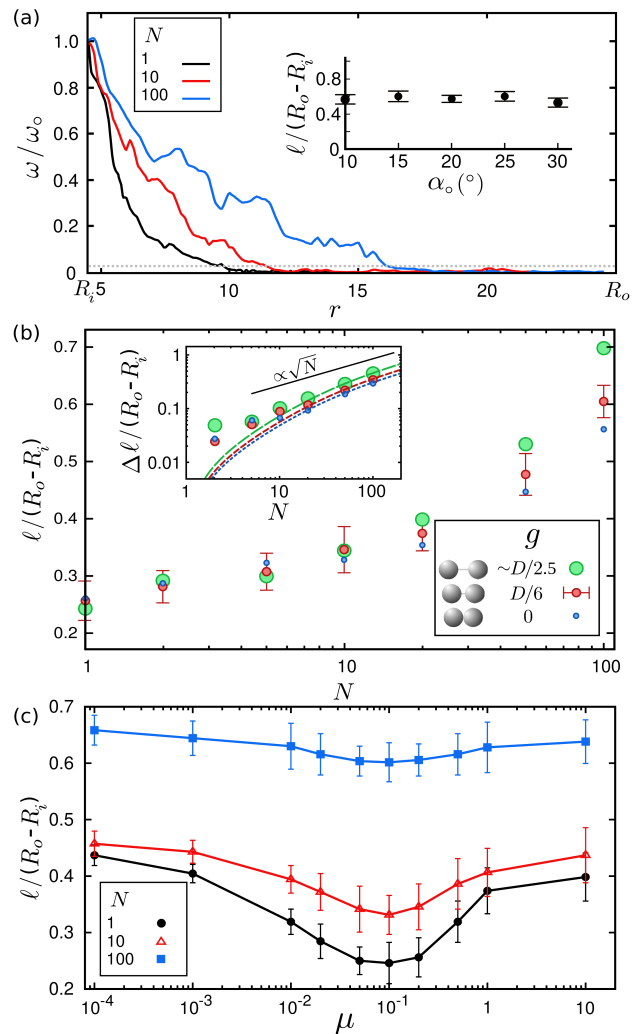


FIG. 2. (a) Mean angular velocity  $\omega$ , scaled by the mean angular velocity of the vane  $\omega_o = 2f\alpha_o$ , vs the radial distance  $r$  from the cylinder axis (in units of  $D$ ) for  $\alpha_o = 20^\circ$ ,  $\mu = 0.2$ , and different chain lengths  $N$ . The dotted line denotes the threshold angular velocity  $\omega_c = 0.03 \frac{\text{rad}}{\text{s}}$ . Inset: Penetration depth  $\ell$  vs the rotation amplitude  $\alpha_o$  for  $N=100$ . (b)  $\ell$  vs  $N$  for different values of the bond length  $g$ . The standard deviation is shown for  $g = \frac{D}{6}$  data as an example. Inset: Excess penetration depth  $\Delta\ell$  vs  $N$ . The dashed lines represent  $\Delta\ell$  obtained via Eq. (1). (c)  $\ell$  vs  $\mu$  for  $g = \frac{D}{6}$  and different  $N$ .

reported in granular materials [42–44]; in contrast, here a wide shear zone forms near the moving boundary. We characterize the size of the shear zone by the penetration depth  $\ell$ , defined as the radial distance from the blade edges at which the angular velocity falls below a threshold value  $\omega_c$  (i.e.  $0 \leq \ell \leq R_o - R_i$ ); see Figs. 1 and 2(a). Here, the results are presented for  $\omega_c = 0.03 \frac{\text{rad}}{\text{s}}$  but our reported trends and conclusions are fairly insensitive to this choice. By varying  $\alpha_o$  from  $10^\circ$  to  $30^\circ$  and repeating the simulations at each  $\alpha_o$  for different initial configurations, we make sure that  $\ell$  is independent of  $\alpha_o$  in the LAOS regime; see, e.g., the inset of Fig. 2(a).

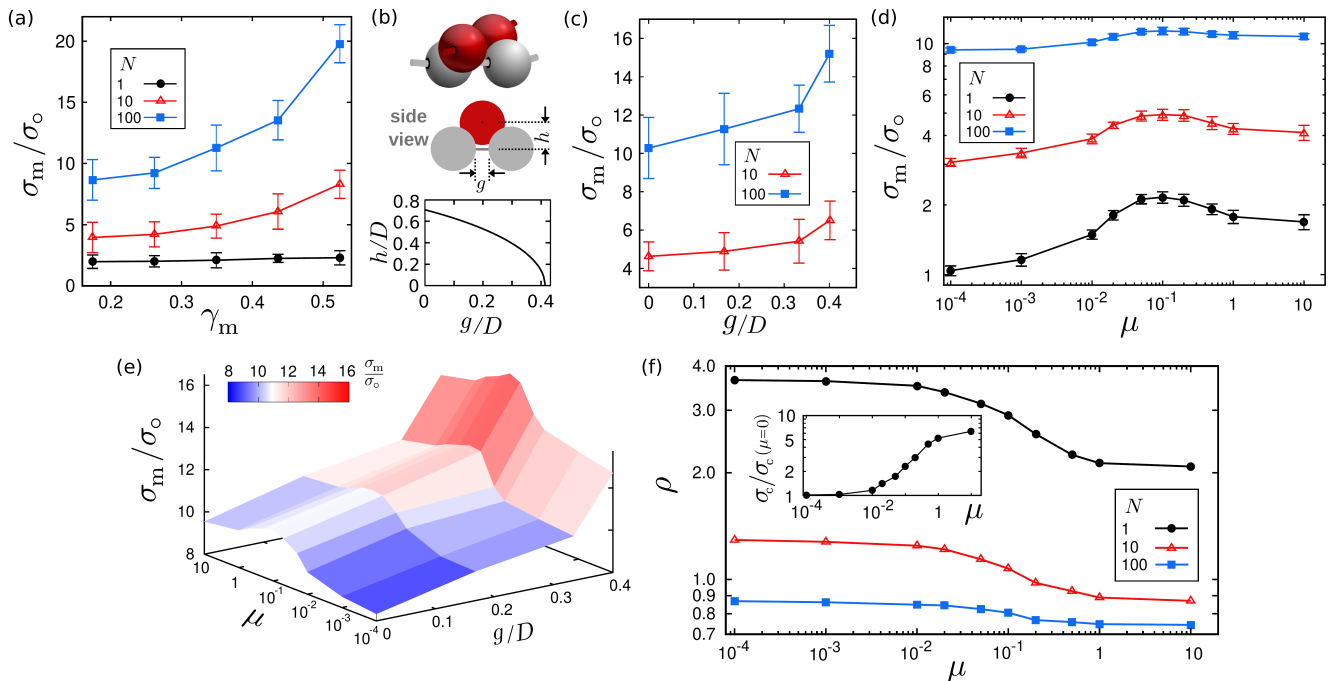


FIG. 3. (a) Maximum normal stress  $\sigma_m$  exerted on the vane, scaled by the similar stress  $\sigma_o$  in a packing with  $\mu=0$  and  $N=1$ , vs the maximum shear strain  $\gamma_m$  ( $\propto \alpha_o$ ) for  $\mu=0.2$  and different chain lengths. (b) Illustration of an interlocking event between the grains of different chains (top) and the minimum possible distance  $h$  between the bonds vs  $g$  (bottom). (c)  $\sigma_m$  vs  $g$  for  $\mu=0.2$ ,  $\alpha_o=20^\circ$ , and different  $N$ . (d)  $\sigma_m$  vs  $\mu$  for  $g=\frac{D}{6}$  and different  $N$ . (e)  $\sigma_m$  in the  $(g, \mu)$  space for  $N=100$ . (f) Contact density  $\rho$  (in units of  $D^{-3}$ ) vs  $\mu$  for different  $N$ . Inset: Critical normal stress  $\sigma_c$  exerted on the vane at the onset of yielding, scaled by  $\sigma_c$  for  $\mu=0$ , vs  $\mu$ . The friction is changed before shearing a static packing of chains with  $N=100$  constructed at  $\mu=0$ .

The dependence of  $\ell$  on  $N$  is shown in Fig. 2(b). The behavior at the small  $N$  regime is mainly dominated by the rheology of individual grain systems (i.e.  $N=1$ ) and  $\ell$  grows slowly with  $N$ ; however, the growth rate increases for long chains. It can be also seen that  $\ell$  varies independently of  $g$  for small  $N$  but systematically increases with  $g$  at the large  $N$  regime. It is known that stress reduction at shear-direction reversals in oscillatory shear of granular assemblies slightly broadens the shear zone up to a few grain diameters [45]. However, formation of wider shear zones in our chain packings is due to the correlated dynamics of rotating chains. For sufficiently long chains, we hypothesize that the penetration depth of the shear deformation roughly scales with the length-scale that the chains in contact with the blade edges extend into the bulk of the system. By calculating the mean end-to-end distance  $\xi$  of a flexible chain of length  $N$  with segment length  $D+g$  and a mean persistence  $p$  in the *Supplemental Material* (see also persistent random walk models [46, 47]) and assuming that  $\ell \propto \xi$ , we obtain

$$\ell \propto \left[ \frac{1+p}{1-p} N + \frac{1}{(1-p)^2} (2p^N + p^2 - 2p - 1) \right]^{0.5} (D+g) \quad (1)$$

for  $N > 1$ , which reduces to  $\ell \propto \sqrt{\frac{1+p}{1-p}} N(D+g)$  in the large  $N$  limit [40]. After subtracting the  $\ell$  of individual grains, we obtain the excess penetration depth

$\Delta\ell = \ell(N) - \ell(N=1)$ , as the pure contribution from the chain structure. The inset of Fig. 2(b) shows that  $\Delta\ell$  extracted from Eq. (1) satisfactorily captures both  $N$  and  $g$  dependence of  $\ell$  in the large  $N$  limit.

Next, we compare  $\ell$  in packings constructed with different coefficients of friction  $\mu$ . Our striking finding is that  $\ell$  develops a minimum at  $\mu \approx 0.1$  for all chain lengths [see Fig. 2(c)]. Thus, the packings constructed with intermediate values of  $\mu$  resist stronger against yielding, leading to smaller shear zones. The effect, however, becomes less pronounced in the large  $N$  limit.

*Mechanical response and strain stiffening.*— By measuring the maximum normal stress  $\sigma_m$  exerted on the vane, we study the role of the key factors on the stress development in granular chain systems. The yield stress of individual grain packings varies negligibly with the rotation amplitude in the LAOS regime, as shown in Fig. 3(a). In contrast, in chain packings with  $N \geq 9$  (i.e. the minimum length required for the formation of full rings), increasing the shear strain strengthens the entanglements through semiloop formation, leading to a pronounced strain stiffening [6, 8]. However, the developed stress is partially due to the interlockings between the grains of different chains. To evaluate the relative contributions of these two types of topological constraints (i.e. semiloops vs interlocking events), we vary the min-

imum possible distance  $h$  between the bonds. This is achieved by varying the gap size  $g$ , which is related to  $h$  via  $h = \sqrt{(D^2 - 2gD - g^2)}/2$ ; see Fig. 3(b). The strength of each interlocking entanglement event grows with increasing  $g$  (decreasing  $h$ ), as it becomes more difficult for the grains to move over each other. Figure 3(c) shows that  $\sigma_m$  can grow even up to 50% upon varying  $g$  from 0 to  $\sim 0.4D$  (We remain in the range  $g \leq g_{\max} = (\sqrt{2}-1)D$ ; otherwise the bonds can touch, which further complicates the behavior). Notably, longer chains develop a larger degree of strain stiffening upon increasing the bond length. Indeed in the large  $N$  limit the majority of the interlocking events occur between different chains: The volume covered by a chain and the volume of its constituent grains scale with  $\xi^3 \sim N^{1.5}$  and  $N$ , respectively; thus, the occupation fraction for each chain decays as  $\sim 1/\sqrt{N}$  and the chain rarely intersects itself in the limit  $N \rightarrow \infty$ .

Similar to the penetration depth, the maximum stress  $\sigma_m$  exhibits a nonmonotonic behavior with the coefficient of friction. Figure 3(d) shows that  $\sigma_m$  reaches a maximum at  $\mu \approx 0.1$ , which indicates again that the assemblies constructed with intermediate values of friction are more stable structures and resist stronger against shear deformations. Figure 3(e) summarizes the stress response of a granular chain packing in the  $(g, \mu)$  space.

To understand the intriguing behavior as a function of  $\mu$ , the crucial point to note is that each value of  $\mu$  is accompanied by a different granular-chain packing structure because the packings are newly generated for each value of  $\mu$  (These structures differ from the frictional fiber assemblies generated by other protocols [48, 49]). It is known that frictional random packings of individual grains are hyperstatic structures in which the mean coordination number  $z$  undergoes a transition with  $\mu$  [26, 50–52]. Since the stress tensor components in a random granular packing are proportional to the density of the interparticle contacts  $\rho = z\phi/2V_g$  (with  $\phi$  and  $V_g$  being the packing fraction and grain volume, respectively) [53, 54], here we measure  $\rho$  as a function of  $\mu$  in chain packings. As shown in Fig. 3(f),  $\rho$  exhibits plateaus at high and low friction limits and shows a smooth and

monotonic transition in between. We hypothesize that the nonmonotonic mechanical response results from two competing effects: while increasing  $\mu$  lowers the connectivity of the contact network, it strengthens the structure by providing larger local freedom for the tangential forces. The  $\rho$ - $\mu$  transition is shallower in assemblies with longer chains, which explains why the non-monotonicity of the mechanical response is less pronounced in the large  $N$  limit. In support of our hypothesis, we measure the response of the same structure for different values of  $\mu$ . In this way, the role of connectivity is switched off and  $\mu$  should solely strengthen the response. We take a static frictionless packing of chains with  $N=100$ , change the value of friction, and exert an increasing normal stress on the vane to bring the packing to the onset of yielding. By repeating this procedure for different values of  $\mu$ , we find that the critical yield stress  $\sigma_c$  exerted on the vane grows monotonically with  $\mu$  [inset of Fig. 3(f)].

*Nonlinear rheology.*— After applying many cycles of oscillatory shear to reach the steady state, we analyze the stress-strain relation in one shear cycle to clarify how the evolution of the contributions of shear strain  $\gamma$  and shear rate  $\dot{\gamma}$  depend on  $g$  and  $\mu$ . The elastic Lissajous curves presented in Fig. 4 show that the rheological response is highly nonlinear, i.e., higher harmonics are present in the signal. The degree of intercycle stiffening slightly increases with  $g$  [see Fig. 4(a)]; thus, elastic stresses grow with the bond length. In contrast, viscous stresses develop with increasing  $\mu$  leading to wider Lissajous curves [Fig. 4(b)]. This can be quantified by the dimensionless loss tangent,  $\tan(\delta)$ , which represents the ratio of dissipated to stored energy in one cycle. Figure 4(c) reveals that the rate of energy dissipation first increases with  $\mu$  but slows down in the large  $\mu$  limit, presumably due to weak network connectivity at large coefficients of friction. Interestingly,  $\tan(\delta)$  is highly correlated to the yield stress [Fig. 4(c)-inset], suggesting that the yield point can be predicted from, e.g., the complex shear modulus.

In summary, our results demonstrate that the physics of packings of entangled granular chains differs from that of molecular polymer systems. The intriguing role of friction in complex assemblies of long semiflexible objects can have possible implications for design of new smart textiles and disordered meta materials [15–22]. Understanding the structure and dynamics of externally-driven interacting filamentous assemblies can be also insightful for packaging optimization problems [55, 56] and has a high potential for technological applications. Although interlocking constraints exist between polymer chains with irregular structures, our results show that the regular gaps between the grains in commercial granular chains can significantly affect the strength of entanglements and the rheological response of the system. Understanding the interplay of entanglements and friction is a key to answer how entangled systems of macroscale long objects yield and flow.

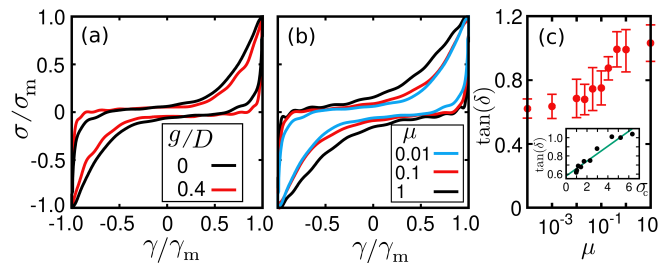


FIG. 4. Elastic Lissajous plots for  $N=100$ ,  $\gamma_m \simeq 0.35$  and (a)  $\mu = 0.01$  and different bond lengths, and (b)  $g=0$  and different values of  $\mu$ . (c) Loss tangent vs  $\mu$  in packings with  $g=0$ . Inset:  $\tan(\delta)$  vs yield stress  $\sigma_c$ . The line represents a linear fit.

M.R.S. acknowledges support by the Young Investigator Grant of the Saarland University, Grant No. 7410110401 and by the Deutsche Forschungsgemeinschaft

(DFG) through Collaborative Research Center SFB 1027. M.H. acknowledges funding from the Netherlands Organization for Scientific Research through NWO-VIDI grant No. 680-47-548/983.

### Appendix: Calculation of the mean end-to-end distance of a flexible chain

In order to calculate the mean end-to-end distance  $\xi$  of a flexible chain of length  $N$  with bond length  $D+g$ , we first consider the problem in two dimensions (see Fig. 5). Assuming that the first grain of the chain is located at the origin in an arbitrary Cartesian frame, the angle of the first bond with the  $x$ -axis,  $\theta_1$ , can be represented as a random angle with an isotropic distribution  $P(\theta_1)=\frac{1}{2\pi}$ . However, the next successive local orientations of the chain are correlated since the next bond angles  $\theta_i$  are limited to uniformly vary within the  $-\theta_{\max} \leq \theta_i \leq \theta_{\max}$  range, i.e., the bond-angle distribution is  $P(\theta_i)=\frac{1}{2\theta_{\max}}$  for  $i \geq 2$ . The directional changes of the chain can be modeled as a persistent random walk, i.e., a stochastic motion with a preference to move along the arrival direction [46, 47]. We quantify the mean directional persistence of the chain with  $p = \langle \cos \theta \rangle = \int d\theta P(\theta) \cos(\theta)$ , which varies from  $p=1$  for a straight rod-like chain to lower values ( $1 < p \leq 0$ ) for flexible chains.

By projecting each bond along the  $x$ -axis, the  $x$ -coordinate of the  $N$ -th grain center is given as

$$x = (D+g) \sum_{i=1}^{N-1} \cos \alpha_i, \quad (2)$$

where  $\alpha_i$  is the  $i$ -th bond angle with the  $x$ -axis, given as  $\alpha_i = \theta_1 + \dots + \theta_i$ . Using the uniform distributions  $P(\theta_1)$  and  $P(\theta_i)$  (for  $i \geq 2$ ), the ensemble-averaged  $x$ -coordinate of the  $N$ -th grain,  $\langle x \rangle$ , can be obtained as

$$\langle x \rangle = (D+g) \sum_{i=1}^{N-1} \int_{-\theta_{\max}}^{\theta_{\max}} d\theta_i P(\theta_i) \dots \int_{-\theta_{\max}}^{\theta_{\max}} d\theta_2 P(\theta_2) \int_{-\pi}^{\pi} d\theta_1 P(\theta_1) \cos(\theta_1 + \dots + \theta_i) = 0, \quad (3)$$

because the integral over  $\theta_1$  vanishes.

Next, we calculate the second moment of displacement of the  $N$ -th grain,  $\langle x^2 \rangle$ . Using Eq. (2),  $\langle x^2 \rangle$  reads

$$\langle x^2 \rangle = (D+g)^2 \left\langle \sum_{i=1}^{N-1} \sum_{j=1}^{N-1} \cos \alpha_i \cos \alpha_j \right\rangle = (D+g)^2 \left\langle \sum_{i=1}^{N-1} \cos^2 \alpha_i + 2 \sum_{i>j} \cos \alpha_i \cos \alpha_j \right\rangle. \quad (4)$$

The ensemble average of the first term leads to

$$(D+g)^2 \sum_{i=1}^{N-1} \langle \cos^2 \alpha_i \rangle = (D+g)^2 \sum_{i=1}^{N-1} \int_{-\theta_{\max}}^{\theta_{\max}} d\theta_1 P(\theta_1) \dots \int_{-\theta_{\max}}^{\theta_{\max}} d\theta_2 P(\theta_2) \int_{-\pi}^{\pi} d\theta_1 P(\theta_1) \cos^2(\theta_1 + \dots + \theta_i) = \frac{N-1}{2} (D+g)^2, \quad (5)$$

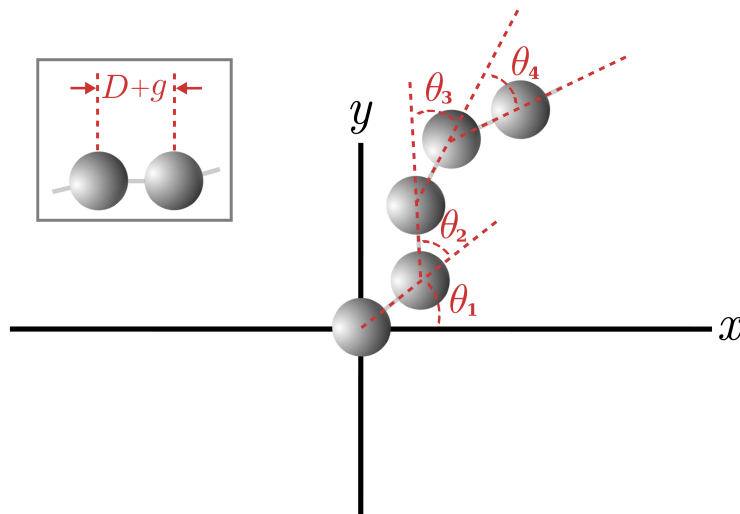


FIG. 5. Schematic of a few first grains of a granular chain. The initial angle with the  $x$ -axis and the successive bond angles are denoted with  $\theta_1$  and  $\theta_i$  ( $i \geq 2$ ), respectively.

and the second term of Eq.(4) can be evaluated as

$$\begin{aligned}
& 2(D+g)^2 \sum_{i>j} \langle \cos \alpha_i \cos \alpha_j \rangle \\
&= 2(D+g)^2 \sum_{i=1}^{N-1} \sum_{j=1}^{i-1} \int_{-\theta_{\max}}^{\theta_{\max}} d\theta_1 P(\theta_1) \cdots \int_{-\theta_{\max}}^{\theta_{\max}} d\theta_2 P(\theta_2) \int_{-\pi}^{\pi} d\theta_1 P(\theta_1) \cos(\theta_1 + \cdots + \theta_i) \cos(\theta_1 + \cdots + \theta_j) \\
&= (D+g)^2 \sum_{i=1}^{N-1} \sum_{j=1}^{i-1} \int_{-\theta_{\max}}^{\theta_{\max}} d\theta_1 P(\theta_1) \cdots \int_{-\theta_{\max}}^{\theta_{\max}} d\theta_{j+1} P(\theta_{j+1}) \cos(\theta_{j+1} + \cdots + \theta_i) \\
&= (D+g)^2 \sum_{i=1}^{N-1} \sum_{j=1}^{i-1} \left( \int_{-\theta_{\max}}^{\theta_{\max}} d\theta P(\theta) \operatorname{Re}[e^{i\theta}] \right)^{i-j} \\
&= (D+g)^2 \sum_{i=1}^{N-1} \sum_{j=1}^{i-1} p^{i-j} = (D+g)^2 \frac{p}{1-p} \left[ N-1 - \frac{1-p^{N-1}}{1-p} \right].
\end{aligned} \tag{6}$$

Similar results as Eqs.(4)-(6) can be obtained for  $\langle y^2 \rangle$  due to symmetry. Hence, we obtain the following expression for the mean end-to-end distance of a flexible chain

$$\xi = \sqrt{\langle x^2 \rangle + \langle y^2 \rangle} = (D+g) \left[ \frac{1+p}{1-p} N + \frac{1}{(1-p)^2} (2p^N + p^2 - 2p - 1) \right]^{0.5} \tag{7}$$

for  $N > 1$ . This equation reduces to  $\xi = \sqrt{\frac{1+p}{1-p} N (D+g)}$  in the large  $N$  limit [40]. Although extension of the above approach to three dimensions is possible, a more systematic formalism to calculate the moments of displacement of a persistent random walk via a Fourier-z-transform technique was previously developed in [57, 58]. Following this approach, it can be verified that the same expression for  $\xi$  as for the 2D solution presented in Eq.(7) holds in 3D, however, with replacing the previous definition of the directional persistence  $p$  in 2D with  $p = \int d\theta \sin(\theta) P(\theta) \cos(\theta)$ . The approach can be also extended to multi-state persistent random walks [59], which is applicable to the case of dealing with a non-uniform directional persistence along a flexible chain.

- 
- [1] M. Rubenstein and R. H. Colby, *Polymer Physics* (Oxford University Press, New York, 2003).
- [2] C. J. O. Reichhardt and L. M. Lopatina, *Science* **326**, 374 (2009).
- [3] L. N. Zou, X. Cheng, M. L. Rivers, H. M. Jaeger, and S. R. Nagel, *Science* **326**, 408 (2009).
- [4] K. Safford, Y. Kantor, M. Kardar, and A. Kudrolli, *Phys. Rev. E* **79**, 061304 (2009).
- [5] F. Samadi Taheri, H. Fazli, M. Doi, and M. Habibi, *Soft Matter* **14**, 5420 (2018).
- [6] E. Brown, A. Nasto, A. G. Athanassiadis, and H. M. Jaeger, *Phys. Rev. Lett.* **108**, 108302 (2012).
- [7] D. Dumont, M. Houze, P. Rambach, T. Salez, S. Patinet, and P. Damman, *Phys. Rev. Lett.* **120**, 088001 (2018).
- [8] M. R. Shaebani, G. Giménez-Ribes, S. Zondervan, L. M. C. Sagis, E. van der Linden, and M. Habibi, arXiv: 2208.13516 (2022).
- [9] P. S. Sarate, T. G. Murthy, and P. Sharma, *Soft Matter* **18**, 2054 (2022).
- [10] L. R. Gómez, N. A. Garcia, and T. Poschel, *Proc. Natl. Acad. Sci. USA* **117**, 3382 (2020).
- [11] E. Ben-Naim, Z. A. Daya, P. Vorobieff, and R. E. Ecke, *Phys. Rev. Lett.* **86**, 1414 (2001).
- [12] L. M. Lopatina, C. J. Olson Reichhardt, and C. Reichhardt, *Phys. Rev. E* **84**, 011303 (2011).
- [13] B. W. Soh, I. R. Gengaro, A. R. Klotz, and P. S. Doyle, *Phys. Rev. Res.* **1**, 033194 (2019).
- [14] M. Hansell, *Animal Architecture* (Oxford Animal Biology Series, Oxford, 2005), ISBN 0-9538032-0-1.
- [15] B. Aktas, Y. S. Narang, N. Vasios, K. Bertoldi, and R. D. Howe, *Adv. Funct. Mater.* **31**, 2007554 (2021).
- [16] G. Verhille, S. Moulinet, N. Vandenberghe, M. Adda-Bedia, and P. L. Gal, *Proc. Natl. Acad. Sci. USA* **114**, 4607 (2017).
- [17] M. J. Mirzaali, M. Habibi, S. Janbaz, L. Vergani, and A. A. Zadpoor, *Sci. Rep.* **7**, 13028 (2017).
- [18] N. Weiner, Y. Bhosale, M. Gazzola, and H. King, *J. Appl. Phys.* **127**, 050902 (2020).
- [19] Y. J. Yun, W. G. Hong, W.-J. Kim, Y. Jun, and B. H. Kim, *Adv. Mater.* **25**, 5701 (2013).
- [20] H. Sunami, Y. Shimizu, N. Futenma, J. Denda, H. Nakasone, S. Yokota, H. Kishimoto, M. Makita, and Y. Nishikawa, *Adv. Mater. Interfaces* **9**, 2101776 (2022).
- [21] J. Hu, H. Meng, G. Li, and S. I. Ibekwe, *Smart Mater. Struct.* **21**, 053001 (2012).
- [22] S. Poincloux, M. Adda-Bedia, and F. Lechenault, *Phys. Rev. X* **8**, 021075 (2018).
- [23] C. Goldenberg and I. Goldhirsch, *Nature* **435**, 188 (2005).
- [24] M. R. Shaebani, T. Unger, and J. Kertész, *Phys. Rev. E* **76**, 030301 (2007).

- [25] M. R. Shaebani, T. Unger, and J. Kertész, *Phys. Rev. E* **78**, 011308 (2008).
- [26] T. Unger, J. Kertész, and D. E. Wolf, *Phys. Rev. Lett.* **94**, 178001 (2005).
- [27] A. Singh, C. Ness, R. Seto, J. J. de Pablo, and H. M. Jaeger, *Phys. Rev. Lett.* **124**, 248005 (2020).
- [28] S. Ostojic and D. Panja, *Phys. Rev. Lett.* **97**, 208001 (2006).
- [29] A. Fall, B. Weber, M. Pakpour, N. Lenoir, N. Shahidzadeh, J. Fiscina, C. Wagner, and D. Bonn, *Phys. Rev. Lett.* **112**, 175502 (2014).
- [30] K. Farain and D. Bonn, arXiv: 2202.00041 (2022).
- [31] S. H. E. Rahbari, M. Otsuki, and T. Poschel, *Commun. Phys.* **4**, 71 (2021).
- [32] I. Regev and C. Reichhardt, *Phys. Rev. E* **87**, 020201 (2013).
- [33] J. T. Parley, S. Sastry, and P. Sollich, *Phys. Rev. Lett.* **128**, 198001 (2022).
- [34] P. Tapadia, S. Ravindranath, and S. Q. Wang, *Phys. Rev. Lett.* **96**, 196001 (2006).
- [35] M. Baggioli, S. Grieninger, and H. Soltanpanahi, *Phys. Rev. Lett.* **124**, 081601 (2020).
- [36] K. Kamani, G. J. Donley, and S. A. Rogers, *Phys. Rev. Lett.* **126**, 218002 (2021).
- [37] M. Jean, *Comput. Methods Appl. Mech. Eng.* **177**, 235 (1999).
- [38] Z. Shojaaee, M. R. Shaebani, L. Brendel, J. Török, and D. E. Wolf, *J. Comput. Phys.* **231**, 612 (2012).
- [39] M. R. Shaebani, T. Unger, and J. Kertész, *Int. J. Mod. Phys. C* **20**, 847 (2009).
- [40] M. Doi and S. F. Edwards, *The Theory of Polymer Dynamics* (Oxford University Press, Oxford, 1986).
- [41] M. R. Shaebani, R. Jose, L. Santen, L. Stankevics, and F. Lautenschläger, *Phys. Rev. Lett.* **125**, 268102 (2020).
- [42] D. Fenistein and M. van Hecke, *Nature* **425**, 256 (2003).
- [43] R. Moosavi et. al, *Phys. Rev. Lett.* **111**, 148301 (2013).
- [44] M. R. Shaebani, J. Török, M. Maleki, M. Madani, M. Harrington, A. Rice, and W. Losert, *Phys. Rev. Lett.* **127**, 278003 (2021).
- [45] M. Toiya, J. Stambaugh, and W. Losert, *Phys. Rev. Lett.* **93**, 088001 (2004).
- [46] P. Tierno and M. R. Shaebani, *Soft Matter* **12**, 3398 (2016).
- [47] R. Nossal and G. H. Weiss, *J. Theor. Biol.* **47**, 103 (1974).
- [48] A. Ward, F. Hilitski, W. Schwenger, D. Welch, A. W. C. Lau, V. Vitelli, L. Mahadevan, and Z. Dogic, *Nat. Mater.* **14**, 583 (2015).
- [49] V. Negi and R. C. Picu, *Soft Matter* **17**, 10186 (2021).
- [50] M. R. Shaebani, T. Unger, and J. Kertész, *Phys. Rev. E* **79**, 052302 (2009).
- [51] L. E. Silbert, *Soft Matter* **6**, 2918 (2010).
- [52] P. Wang, C. Song, C. Briscoe, K. Wang, and H. A. Makse, *Physica A* **389**, 3972 (2010).
- [53] M. R. Shaebani, M. Madadi, S. Luding, and D. E. Wolf, *Phys. Rev. E* **85**, 011301 (2012).
- [54] M. R. Shaebani, J. Boberski, and D. E. Wolf, *Granular Matter* **14**, 265 (2012).
- [55] R. Vetter, F. K. Wittel, and H. J. Herrmann, *Nat. Commun.* **5**, 4437 (2014).
- [56] M. R. Shaebani, J. Najafi, A. Farnudi, D. Bonn, and M. Habibi, *Nat. Commun.* **8**, 15568 (2017).
- [57] M. R. Shaebani, Z. Sadjadi, I. M. Sokolov, H. Rieger, and L. Santen, *Phys. Rev. E* **90**, 030701 (2014).
- [58] Z. Sadjadi, M. R. Shaebani, H. Rieger, and L. Santen, *Phys. Rev. E* **91**, 062715 (2015).
- [59] M. R. Shaebani and H. Rieger, *Front. Phys.* **7**, 120 (2019).